PerFormer: A Permutation Based Vision Transformer for Remaining Useful Life Prediction

Zhengyang Fan, *Member, IEEE*, Wanru Li, Kuo-Chu Chang, *Life Fellow, IEEE*, Ting Yuan, *Member, IEEE*

***Abstract*—Accurately estimating the remaining useful life (RUL) for degradation systems is crucial in modern prognostic and health management (PHM). Convolutional Neural Networks (CNNs), initially developed for tasks like image and video recognition, have proven highly effectively in RUL prediction, demonstrating remarkable performance. However, with the emergence of the Vision Transformer (ViT), a Transformer model tailored for computer vision tasks such as image classification, and its demonstrated superiority over CNNs, there is a natural inclination to explore its potential in enhancing RUL prediction accuracy. Nonetheless, applying ViT directly to multivariate sensor data for RUL prediction poses challenges, primarily due to the ambiguous nature of spatial information in time series data. To address this issue, we introduce the PerFormer, a permutation-based vision transformer approach designed to permute multivariate time series data, mimicking spatial characteristics akin to image data, thereby making it suitable for ViT. To generate the desired permutation matrix, we introduce a novel permutation loss function aimed at guiding the convergence of any matrix towards a permutation matrix. Our experiments on NASA's C-MAPSS dataset demonstrate the PerFormer's superior performance in RUL prediction compared to state-of-the-art methods employing CNNs, Recurrent Neural Networks (RNNs), and various Transformer models. This underscores its effectiveness and potential in PHM applications.**

***Index Terms*—Deep Learning, Feature Representation, Vision Transformer, Attention, Remaining Useful Life, Permutation Learning**

I. Introduction

THE shift from traditional preventive maintenance to condition-based predictive maintenance (CBPM) has been accelerated by the rapid advancement of modern instruments and sensory technology. These advancements, enable the real-time collection of condition monitoring data from operational degradation systems [1], [2], [3]. This transition to CBPM represents a significant improvement over traditional approaches, empowering organizations to enhance equipment reliability in today's demanding industriallandscapes [4], [5], [6].

Accurately predicting remaining useful life (RUL) in CBPM is of utmost impoerance. RUL prediction plays a pivotal role in optimizing maintenance strategies by offering crucial insights into the anticipated lifespan of essential assets. By estimating the time remaining until the end of a system's operational life cycle, maintenance activities can be strategically planned and executed at optimal intervals, minimizing downtime and reducing costs [7]. This proactive approach ensures that maintenance resources are allocated efficiently, maximizing system performance and reliability while preventing unnecessary disruptions in complex industrial settings [8].

RUL prediction methods can be broadly categorized into two main approaches: model-based methods and data-driven methods. Model-based methods rely on physics-based or mechanistic models that describe the degradation process of the asset over time [9], [10]. For example, when predicting RUL for mechanical components like bearings or gears, model-based methods may involve formulating equations that describe wear, fatigue, or corrosion processes. However, the inherent complexity of real-world degradation systems presents a significant challenge in accurately modeling these processes. As a result, applying model-based methods in practical CBPM systems may lead to suboptimal prediction performance and less effective decisions in maintenance scheduling.

As data volume and computing power continue to suege, coupled with the superior performance of deep learning methods in various domains such as cybersecurity [11], [12], [13] and geology [14], the research emphasis for RUL estimation is shifting from model-based methods to data-driven approaches. A prominent deep learning model, the Convolutional Neural Network (CNN), has achieved remarkable success in image recognition tasks owing to its exceptional feature extraction and object recognition capabilities, thus emerging as the most prevalent architecture in RUL prediction [15], [16], [17], [18], [19], [20], [21], [22], [23], [24].

Recently, the Vision Transformer (ViT) [25], a variant of the classical transformer architecture [26] tailored for vision tasks, has demonstrated superior performance in tasks such as object detection and signal processing [27], [28]. Given its success, it is natural to consider potential enhancements by incorporating ViT into RUL prediction.However, directly applying ViT to predict RUL using multivariate time series sensor data can be challenging due to the ambiguous nature of spatial information within such data. Therefore, in this study, we propose PerFormer, a permutation-based vision transformer, for RUL prediction in degradation systems. The tationale behind incorporating permutation into ViT is illustrated at the top of Figure 1, where rows of an image are randomly permuted. It becomes evident that the resulting performance of ViT with this permuted image can be unsatisfactory, as features such as boundaries and edges in the image are disrupted [29], [30]. To ensure ViT achieves the desired performance on this permuted image, we need to identify the optimal permutation that yields the optimal prediction performance. In this context, the best permutation should be the one that restores the original

Z. Fan and K. Chang are with Department of Systems Engineering and Operations Research, George Mason University

W. Li is with Department of Soil and Environmental Science, University of Wisconsin-Madison

T. Yuan is with Department of XX, Shanghai Jiao Tong University

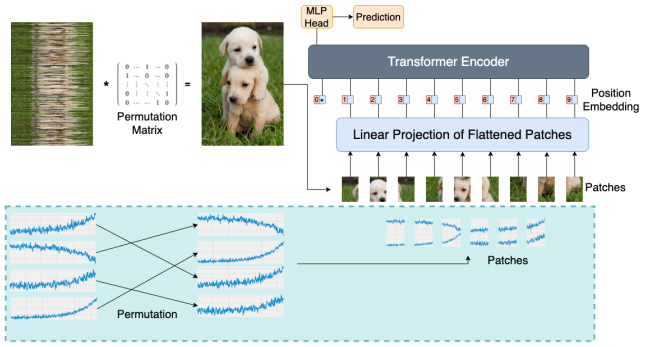

Fig. 1. Motivation of the PerFormer: The motivation behind PerFormer begins with the example shown in the top left corner of an image whose rows are randomly permuted. To extract meaningful feature representations from this image, it's necessary to rearrange the rows back to their original order, creating a restored image suitable for analysis with ViT in subsequent predictive tasks. In a similar manner, we approach multivariate time series sensor readings as though they are images with permuted rows. Our objective is to discover the optimal permutation that yields the best predictive performance when used in conjunction with ViT.

image.

In the proposed PerFormer framework, we conceptualize multivariate time series sensor readings as an image with permuted rows/variables. The goal is to identify the optimal permutation matrix that enhances prediction performance with ViT, as depicted at the bottom of Figure 1.

The contributions of this study can be summarized as follows:

1) We developed a novel ViT-based method for predicting RUL using multivariate time series sensor data as input. To the best of our knowledge, this represents the first attempt to leverage ViT for RUL prediction.
2) Rather than directly applying ViT, we introduced a permutation-based approach that interprets multivariate time series data as a permuted image. Additionally, we proposed a novel loss function designed to guide the outputs of a CNN to converge to a permutation matrix, thereby facilitating the learning of the optimal permutation matrix.
3) Through various numerical experiments conducted on four C-MAPSS turbofan engine datasets, we demonstrated that the performance of our proposed PerFormer method can match that of state-of-the-art RUL prediction algorithms and, in some cases, even surpass them.

The rest of the paper is organized as follows: In Section 2, we conduct a review of relevant literature on RUL prediction using CNNs and Transformers. Section 3 presents a detailed description of the PerFormer model architecture. Section 4 delves into the experimental methodology, including detailed explanations of the experiments, presentation of results, and in-depth analysis. Lastly, Section 5 serves as the conclusion of the paper.

II. Related Works

The application of deep learning techniques, especially CNNs, for estimating RUL for critical components and systems has attracted considerable interest. Li et al. [15] pioneered in demonstrating the efficacy of deep convolutional neural networks for RUL estimation, emphasizing the robustness and accuracy of predictions across diverse prognostic scenarios. Subsequently, Zhu et al. [16] and Jiang et al. [19] further enhanced the CNN framework by incorporating a multiscale feature extraction technique, resulting in a substantial improvement in RUL prediction accuracy for bearings, showcasing the importance of capturing features across different scales. Yang et al. [17] introduced a double-CNN architecture that refined the prediction models by effectively capturing temporal and spatial dependencies within sensor data, leading to more reliable RUL predictions. Cheng et al. [18] extended the CNN methodology by incorporating transfer learning to tackle the complexity of predicting RUL under multiple failure behaviors, demonstrating CNNs adaptability to diverse operational contexts. Wang et al. [20] introduced a deep separable convolutional network that not only lowered the computational burden but also preserved high accuracy, making it suitable for real-time applications in machinery RUL prediction. Further, Kim and Sohn [21] utilized a multitask learning framework within a CNN architecture to concurrently predict RUL and identify health conditions, showcasing the versatility of CNN models in practical applications. Mazaev et al. [22] incorporated a Bayesian approach into the CNN framework to provide uncertainty estimations in RUL predictions. This capability is crucial for decision-making processes in maintenance scheduling, as it allows for a better understanding of the reliability and confidence levels associated with the predicted RUL values. The works of Xu et al. [23] and Chadha et al. [24] introduced dilated convolutional neural networks, which augment the receptive field without losing resolution, proving especially effective in capturing long-range dependencies crucial for accurate RUL estimation. Additionally, prediction methods based on one-dimensional CNNs (1-DCNNs) have also been proposed to improve feature extraction from multivariate time series data, as illustrated in [31], [32].

Recent advancements in RUL prediction increasingly favors Transformer architectures, leveraging attention mechanisms to selectively focus on relevant data segments, thus elevating prediction accuracy and efficiency. Mo et al. [33] introduced a Transformer Encoder integrated with a Gated Convolutional Unit, which significantly improved feature extraction and retention, leading to more precise RUL estimations. Ren et al. [34] developed the DLformer, a Dynamic Length Transformer-based network proficient in handling variable-length data for efficient feature representation in RUL prediction. Meanwhile, Zhang et al. [35] crafted a Trend-Augmented and Temporal-Featured Transformer Network that harnesses multi-sensor signals for robust RUL forecasting. Additionally, Li et al. [36] and Xiang et al. [37] have augmented Transformer-based models with knowledge-driven approaches and uncertainty assessments, respectively, enhancing their predictive capabilities and positioning them as optimal solutions for advanced predictive maintenance. Notably, other studies, such as Zhang et al. [38] and Fan et al. [39], have devised specific attention mechanisms tailored for RUL prediction, such as the DAST and STAR frameworks, which capture both temporal and spatial dynamic. Fan et al. [40] and Chen et al. [41] have

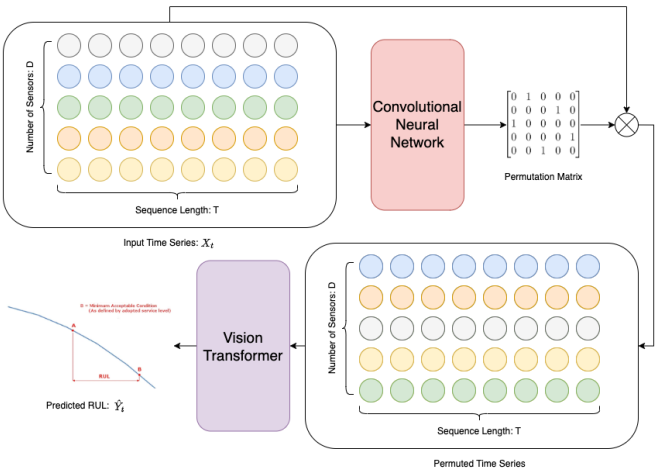

Fig. 2. Workflow of the proposed PerFormer framework

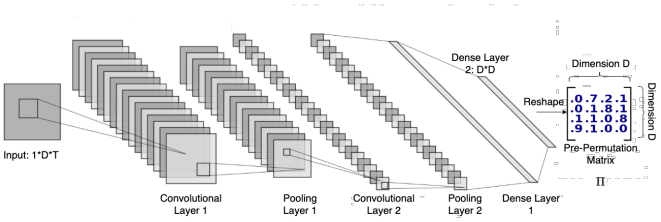

Fig. 3. CNN Architecture for Permutation Learning

also integrated autoencoders with Transformer architectures to create more robust feature representations, thereby enhancing the accuracy of RUL predictions. Unlike these approaches, our proposed PerFormer method employs a ViT, originally designed for spatial data like images and videos with patched data. This signifies a novel direction in handling structured data within the RUL prediction domain.

III. Methodology

In this paper, we aim to predict the RUL of a degradation system based on historical multivariate time series sensor readings denoted as $X_t = x_{t-T+1:t} \in \mathbb{R}^{D\times T}$, where T represents the number of time steps in the input data, and D is the number of onboard sensors. The target output is the predicted RUL $\hat{Y}_t$. Our objective is to predict real-time RUL by establishing the functional relationship between RUL and historical sensor readings, expressed as follows:

$$\hat{Y}_t = f(\Pi(X_t|\theta_1) \cdot X_t|\theta_2) \tag{1}$$

where $\Pi(\cdot|\theta_1)$ is a row permutation matrix modeled using convolutional neural network (CNN) and parameterized by θ_1, and $f(\cdot|\theta_2)$ represents the ViT, which is parameterized by θ_2. Figure 2 shows the general workflow of the proposed PerFormer RUL prediction framework. In the subsequent sections, we elaborate on each element of our proposed PerFormer approach. Starting with the permutation matrix $\Pi(\cdot|\theta_1)$, we introduce a penalty function that designed to transform a given matrix into a permutation matrix in Subsection 3A. Following this, the details of the ViT are discussed in Subsection 3B. Finally, in Subsection 3C, we describe a dynamic penalty weight learning strategy aimed at ensuring the attainment of the desired permutation matrix.

A. Permutation Matrix Learning

A permutation matrix is a square matrix consisting entirely of zeros and exactly one entry of 1 per row and per column, enabling it to perform row and column permutations on any matrix it multiplies. Optimizing this matrix directly within a binary framework poses a challenging non-convex NP problem, akin to integer programming. To facilitate gradient-based learning of the optimal permutation, we employ a convolutional neural network (CNN) to model the permutation matrix, $\Pi(\cdot|\theta_1)$. Figure 3 depicts the CNN network architecture employed in this study for generating permutation matrices. Our CNN model comprises two convolutional layers, two max pooling layers, and two fully connected dense layers. The output dimension of the final fully connected dense layer is D^2, where D represents the number of onboard sensors. To obtain the desired permutation matrix, it is necessary to reshape the output into a matrix of size $D \times D$. However, it is important to note that this $D \times D$ output matrix of CNN is not a permutation matrix since it is not binary valued. Next, we will introduce a method that encourage the output of the CNN to be a permutation matrix.

Let $\Pi_{i,j}(X_t|\theta_1)$ denote the entry in the i-th row and j-th column produced by the CNN after reshaping. For notational simplicity, we use Π and $\Pi_{i,j}$ represent the overall output and individual elements from the CNN, respectively. To transform Π into a permutation matrix, we first apply a row normalization defined by:

$$R_{i,j}(\Pi) = \frac{\exp(\Pi_{i,j})}{\sum_{k=1}^{D} \exp(\Pi_{i,k})} \tag{2}$$

This process results in a matrix $R(\Pi)$, where each row sums to 1 and contains only non-negative values, allowing us to interpret each row as a probability distribution of a random variable. Let Z_i denote the corresponding random variable for i-th row of matrix $R(\Pi)$. To force binary values in the matrix $R(\Pi)$, we can constrain the distributions to be degenerate and we introduce entropy into the optimization process.

Entropy, in probability theory, serves as a measure of the unpredictability in a distribution, calculated by:

$$H(Z_i) = -\sum_{j=1}^{D} R_{i,j}(\Pi) \cdot \log(R_{i,j}(\Pi)) \tag{3}$$

where $H(Z_i)$ denotes the entropy of the distribution represented by row i of matrix $R(\Pi)$. A distribution is degenerate when it consists of a single probable outcome and zero elsewhere, corresponding to an entropy of zero. Thus, we include the following loss function to drive this outcome:

$$L = L_{pred} + \sum_{i=1}^{D} \lambda_i \cdot \left(-\sum_{j=1}^{D} R_{i,j}(\Pi) \cdot \log(R_{i,j}(\Pi)) \right) \tag{4}$$

where L_{pred} denotes the prediction loss, calculated as the mean squared error across N samples:

$$L_{pred} = \frac{1}{N}\sum_{t=1}^{N} \|Y_t - \hat{Y}_t\|_2 \tag{5}$$

Here, λ_i are positive weights that, through the minimization of L, compel each row of $R(\Pi)$ towards a degenerate distribution. However, this transformation doesn't ensure that each column sums to one. Therefore, we introduce an additional penalty term to ensure column normalization in our loss function:

$$L = L_{pred} + \sum_{i=1}^{D} \lambda_i \cdot \left(-\sum_{j=1}^{D} R_{i,j}(\Pi) \cdot \log(R_{i,j}(\Pi)) \right) + \sum_{j=1}^{D} \gamma_j \cdot \left(\|1 - \sum_{i=1}^{D} R_{i,j}(\Pi)\|_2 \right) \tag{6}$$

By incorporating these two sets of penalty functions into the objective function, the resulting matrix $R(\Pi)$ becomes the desired permutation matrix. By left-multiplying this permutation matrix with the original time series input X_t, one can derive the permuted time series, which can then be fed into a ViT for RUL prediction.

B. Vision Transformer

In recent years, ViTs have emerged as a potent architecture in the realm of computer vision, offering a novel approach to image processing and understanding. Unlike traditional CNNs, which have long been dominant in image analysis tasks, ViTs rely solely on self-attention mechanisms, making them particularly adept at capturing global dependencies within images. In this work, we treat the permuted multivariate time series sensory readings as an image and feed it into ViT for RUL predictions. The ViTs mainly consisted of a patch embedding layer, a positional encoding layer, a transformer encoder, and a prediction head.

In patch embedding layer, the permuted multivariate time series is divided into fixed size non-overlapping patches as shown in Figure 1. Each patch is then linearly transformed into a lower-dimensional representation using a trainable linear projection. If we denote the input permuted multivariate time series as X_t of size $D \times T \times 1$ (number of sensors D, sequence length T and a single channel), and we extract patches of size $p \times q$, then the number of patches with be $\frac{D \times T}{p \times q}$. Before feeding the sequence of patches into the encoder, it is linearly projected into a vector of the model dimension d using a learned embedding matrix E. The embedded representations are then concatenated together along with a learnable prediction token x_{pred} that is required to perform the prediction task. The embedded image patches are viewed by the Transformer as a set of patches without any notion of their order. To preserve the spatial arrangement of the patches as in the original image, positional information E_{pos} is encoded and added to the patch representations. The resulting embedded sequence of patches with the token z_0 is given as

$$z_0 = [x_{pred}; x_1E; x_2E; ...; x_nE] + E_{pos} \tag{7}$$

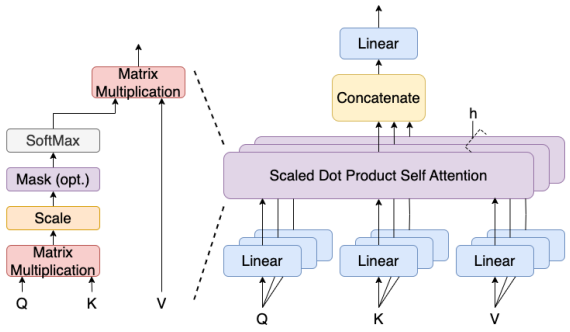

Fig. 4. Multihead Self-Attention

where $E \in \mathbb{R}^{(p\times q)\times d}$ and $E_{pos} \in \mathbb{R}^{(n+1)\times d}$. The sequence of embedded patches z_0 is passed through the Transformer encoder, consisting of L identical layers. Each layer contains two primary components: a multihead self-attention block (MSA) and a fully connected feed-forward dense block (MLP). The MSA block within the encoder is crucial in the Transformer architecture, tasked with determining the relative importance of each patch embedding within the sequence using a self-attention mechanism. This mechanism computes attention scores between different patches to capture dependencies and relationships. The attention scores are calculated as:

$$Attention(Q, K, V) = softmax\left(\frac{QK^T}{\sqrt{d_k}}\right) \cdot V \tag{8}$$

Here, Q, K and V are query, key, and value matrices derived from patch embeddings, and d_k is the dimension of the key vectors. To enhance model expressiveness, self-attention is often computed with multiple heads, allowing the model to concurrently attend to different parts of the input space. In the multi-head attention mechanism, computation is parallelized across h attention heads, each equipped with distinct learned linear projections of the input matrices Q, K and V. The output from each attention head i is computed as:

$$head^i = Attention(QW_Q^i, KW_K^i, VW_V^i) \tag{9}$$

Finally, the outputs from all attention heads are concatenated and linearly transformed to produce the final output of the MSA block:

$$MSA(Q, K, V) = Concat(head^1, head^2, ..., head^h) \cdot W_o \tag{10}$$

Here, W_Q^i, W_K^i, W_V^i and W_o are all learnable weights. The working process of the multihead self-attention function is visualized in Figure 4.

The subsequent MLP block consists of two dense layers with a GELU activation function in between. Both the MSA and MLP blocks of the encoder incorporate residual skip connections and are preceded by a layer normalization (LN) step. The computation for each layer ℓ in the encoder can be expressed as:

$$z'_\ell = MSA(LN(z_{\ell-1})) + z_{\ell-1}, \quad \ell = 1, 2, ..., L \tag{11}$$

$$z_\ell = MLP(LN(z'_\ell)) + z'_\ell, \quad \ell = 1, 2, ..., L \tag{12}$$

In the above equations:

- z_l' represents the output after applying the MSA block followed by layer normalization and adding the residual connection z_{l-1}.
- z_l denotes the final output after passing through the MLP block, layer normalization, and adding the residual connection z_l'.

At the last layer L of the encoder, we extract the first element of the sequence z_L^0 and pass it through a layer normalization for prediction of the RUL:

$$\hat{Y} = LN(z_L^0) \tag{13}$$

C. Dynamic Penalty Weight Adjustment Strategy

In this study, we seek to optimize the following problem for our proposed permutation matrix and ViT predictor:

$$\begin{aligned}\min_{\theta_1,\theta_2} \frac{1}{N}\sum_{t=1}^{N} &\|Y_t - f(R(\Pi(X_t|\theta_1))\cdot X_t|\theta_2)\|_2 \\ &+ \sum_{i=1}^{D}\lambda_i \cdot \left(-\sum_{j=1}^{D} R_{i,j}(\Pi)\cdot\log(R_{i,j}(\Pi))\right) \\ &+ \sum_{j=1}^{D}\gamma_j \cdot \left(\|1-\sum_{i=1}^{D} R_{i,j}(\Pi)\|_2\right)\end{aligned} \tag{14}$$

To ensure that the matrix $R(\Pi(X_t|\theta_1))$ effectively becomes a permutation matrix, setting the penalty weights λ_i and γ_j sufficiently large could theoretically suffice. However, such an approach risks the stochastic gradient descent algorithm producing a non-optimal permutation matrix for RUL prediction by heavily relying on the CNN-based initial permutation network $\Pi(X_t|\theta_1)$. This occurs because high penalty weights could prematurely fix the matrix to its initial state, thereby, ignoring the quality of RUL prediction and stifling exploration of potentially better permutation matrices. This happens due to gradients vanishing once $R(\Pi(X_t|\theta_1))$ solidifies into a permutation matrix.

To circumvent this, we introduce a dynamic penalty weight adjustment strategy, uniformly setting $\lambda = \lambda_i = \lambda_{i'}$ for any $i, i' = 1, 2, ..., D$ and $\gamma = \gamma_j = \gamma_{j'}$ for any $j, j' = 1, 2, ..., D$. We start with $\lambda = \gamma = 0$ at the onset of the training process. Throughout successive epochs, indexed by s, we incrementally increase the weights λ^s and γ^s. Starting with smaller weights allows the initial focus to be on discovering a matrix $R(\Pi(X_t|\theta_1))$ that enhances RUL prediction. As the weights increase in subsequent epochs, the matrix obtained from earlier epochs serves as a starting point. This gradual increase in penalty weights allows for a more balanced exploration of the solution space, preventing premature fixation on suboptimal solutions while still incorporating the benefits of the initial permutation matrix. This process also ensures that $R(\Pi(X_t|\theta_1))$ eventually evolves into a true permutation matrix, which not only meets the structural requirements but also improves prediction accuracy for the RUL task. Let S denote the total number of epochs in the training phase. In our study, we implement the following rule for updating the penalty weights during numerical experiments:

$$\lambda^s = U_\lambda \cdot \frac{T_\lambda \cdot (s \ / \ T_\lambda)}{S}, \quad s = 0, 1, ..., S-1$$
$$\gamma^s = U_\gamma \cdot \frac{T_\gamma \cdot (s \ / \ T_\gamma)}{S}, \quad s = 0, 1, ..., S-1$$

Here, / represents the quotient operator, T_λ and T_γ represent the update rates for λ and γ respectively, while U_λ and U_γ are the upper bounds for these weights. This updating mechanism allows for a gradual increase in the penalty weights over the course of the training iterations, guided by predefined cycles and upper limits.

TABLE I
PARAMETERS OF THE C-MAPSS DATASET

Dataset	FD001	FD002	FD003	FD004
No. of Training Trajectories	100	260	100	249
No. of Testing Engines	100	259	100	248
No. of Operating Conditions	1	6	1	6
No. of Fault Modes	1	1	2	2

IV. EXPERIMENTS

In the upcoming subsections, we will first introduce the CMAPSS dataset used in our experiments and discuss the data preprocessing methods in Section 4A. Following that, Section 4B will elaborate on the performance metrics used to assess the proposed PerFormer framework. Section 4C will delve into the details of hyperparameter tuning and implementation specifics. In Section 4D, we will present the performance results of the PerFormer framework and compare them with state-of-the- art RUL prediction methods. Section 4E will provide a detailed analysis of the performance of PerFormer. Finally, in Section 4F, a set of ablation study will be presented to demonstrate the importance of each component of the PerFormer framework.

A. Data and Preprocessing

For our analysis, we utilized the NASA Commercial Modular Aero-Propulsion System Simulation (CMAPSS) dataset, which serves as a comprehensive benchmark for evaluating the robustness of predictive models concerning RUL of turbofan engines. The CMAPSS dataset is divided into four distinct subdatasets: FD001, FD002, FD003, and FD004, each designed to address different engine behaviors under various operating conditions and fault types as shown in Table I. FD001 and FD003 are each subjected to a single operating condition with one and two fault types, respectively, whereas FD002 and FD004 are tested under six distinct operating conditions, each with one and two fault types, respectively.

Each engine cycle in the dataset is monitored by 21 sensors that record data such as temperatures, pressures, speeds, and other relevant parameters, which are crucial for monitoring the engine's health status. However, not all the sensors significantly contribute to the estimation of the RUL of the engines. Following the approach outlined in [33], we selectively incorporate data from 14 sensors (sensors 2, 3, 4, 7, 8, 9, 11, 12,

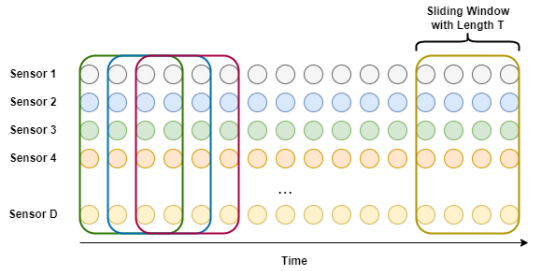

Fig. 5. Illustration of Sliding Window

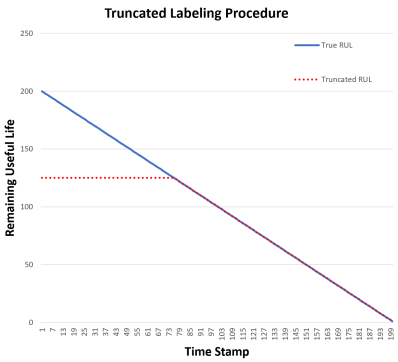

Fig. 6. Truncated RUL of C-MAPSS dataset, $RUL_{max} = 125$ [40]

13, 14, 15, 17, 20, 21) into our training and testing processes. Hence, sensors that showed constant readings throughout the operational lifecycle were excluded to reduce computational complexity and improve model efficiency.

Given the disparate numerical ranges of the sensor measurements, we applied a min–max normalization technique to scale the data. This normalization is expressed mathematically as

$$x' = \frac{x - x_{min}}{x_{max} - x_{min}}$$

where x represents the original sensor readings, and x_{min} and x_{max} are the minimum and maximum values recorded by the sensors respectively.

To effectively model the temporal progression of engine health, we apply a sliding window technique to the time series sensor data. As shown in Figure 5, this approach involves creating overlapping windows of sensor data across consecutive time steps, which helps in capturing the temporal dependencies essential for accurate RUL prediction. Each window aggregates data from a predefined number of cycles, T, sliding over the entire life cycle of the engine.

Our RUL labeling strategy deviates from traditional linear decrease assumptions by adopting a truncated linear model, which more accurately reflects the varying degrees of degradation throughout different life cycle phases of a system. As depicted in Figure 6, initial RULs maintain a constant value, RUL_{max}, representing minimal early degradation, before transitioning into a phase of linear decline as the system approaches failure. This approach ensures that the labels for RUL better mirror the actual progression of system health, capturing the dynamic nature of engine degradation in our dataset.

B. Evaluation Metric

In evaluating the predictive performance of the proposed model for the RUL, two key metrics are employed: the RMSE and an effectiveness Score. The RMSE is a widely accepted metric for evaluating prediction models, particularly in RUL estimation, as it quantifies the averaged magnitude of the prediction error across all samples. Defined mathematically in our study as

$$RMSE = \sqrt{\frac{\sum_{i=1}^{N}(y_i - \hat{y}_i)^2}{N}}$$

TABLE II
HYPERPARAMETERS DESCRIPTION AND BEST HYPERPARAMETER CONFIGURATION

Parameter	FD001	FD002	FD003	FD004
Embedding Dim	64	128	64	128
Hidden Dim	32	32	32	32
Heads in MSA	2	2	2	4
Transformer Layers	1	2	1	2
Temporal Patch Size	2	4	4	2
Spatial Patch Size	7	7	7	7
Sequence Length	32	48	32	48

This metric treats underestimations and overestimations equally. This symmetry ensures that our model's accuracy is evaluated comprehensively, penalizing any deviation from the true RUL values, regardless of its direction. Thus, a lower RMSE value indicates a higher precision of the model in predicting the exact time until a system fails, making it invaluable for comparing our approach with other state-of-the-art methods.

On the other hand, the Effectiveness Score introduces a nuanced layer of assessment by applying different penalty weights based on the direction of the prediction error, recognizing that not all errors are equal in their consequences. This score is calculated using the formula

$$Score = \begin{cases} \sum_{i=1}^{N} e^{-\left(\frac{y_i - \hat{y}_i}{13}\right)} - 1, & \text{if } y_i - \hat{y}_i < 0 \\ \sum_{i=1}^{N} e^{-\left(\frac{y_i - \hat{y}_i}{10}\right)} - 1, & \text{otherwise} \end{cases}$$

C. Hyperparameters Tuning

The hyperparameter tuning process for the proposed PerFormer model involves a grid search aimed at identifying the optimal configuration in terms of RMSE. This grid search covers critical hyperparameters including the embedding dimension, hidden dimension, number of heads in the multi-head self-attention (MSA) mechanism, number of Transformer layers, temporal patch size, spatial patch size, and sequence length. The best parameters configurations for each dataset from FD001 to FD004 are provided in Table II. Our networks are trained using the Adam optimizer with a fixed epoch count of 300. The learning rate is set to 0.0002, while employing a batch size of 64 and a weight decay of 0.05.

TABLE III
RMSE PERFORMANCE COMPARISON. THE BOLD NUMBER REPRESENTS THE BEST MODEL, WHILE THE UNDERSCORE NUMBER REPRESENTS THE SECOND-BEST MODEL.

Method	FD001	FD002	FD003	FD004
SVR	20.96	42.00	21.05	45.35
RF	17.91	29.59	20.27	31.12
GB	15.67	29.09	16.84	29.01
1D-CNN	12.61	22.36	12.64	23.31
2D-CNN	18.45	30.29	19.82	29.16
MHN	12.17	21.06	11.15	22.67
LSTM	16.14	24.49	16.18	28.17
BiLSTM	13.65	23.18	13.74	24.86
BiGRUAE	13.68	20.81	15.53	27.31
CNN-LSTM	14.40	27.23	14.32	26.69
CNN-BiLSTM	13.18	19.09	13.75	20.97
DATCN	11.78	16.95	11.56	18.23
1D-CNN-BiGRU	12.99	16.10	12.48	18.29
AGCNN	12.42	19.43	13.39	21.50
GCT	11.27	22.81	11.42	24.86
DAST	11.43	<u>15.25</u>	11.32	18.32
BiLSTM-DAE Transformer	<u>10.98</u>	16.12	<u>11.14</u>	<u>18.15</u>
STFA	11.35	19.17	11.64	21.41
CDSG	11.26	18.13	12.03	19.73
Proposed Method	**10.91**	**13.97**	**10.70**	**15.78**

TABLE IV
SCORE PERFORMANCE COMPARISON. THE BOLD NUMBER REPRESENTS THE BEST MODEL, WHILE THE UNDERSCORE NUMBER REPRESENTS THE SECOND-BEST MODEL.

Method	FD001	FD002	FD003	FD004
SVR	-	-	-	-
RF	-	-	-	-
GB	-	-	-	-
1D-CNN	273.70	10412	284.10	12466
2D-CNN	1286.70	13570	1596.20	7886.40
MHN	-	-	-	-
LSTM	338	4450	852	5550
BiLSTM	295	4130	317	5430
BiGRUAE	284	2454	428	4707
CNN-LSTM	290	9869	316	6594
CNN-BiLSTM	302.28	1557.56	381.37	3858.78
DATCN	229	1842	257	2317
1D-CNN-BiGRU	223.30	1201.35	268.83	2304.08
AGCNN	225	1492	227	3392
GCT	-	-	-	-
DAST	203	**924**	**154**	<u>1490</u>
BiLSTM-DAE Transformer	**169**	2937	252	3840
STFA	194.44	2493.09	224.53	2760.13
CDSG	188	1740	218	2332
Proposed Method	<u>171.77</u>	<u>1066.30</u>	<u>191.44</u>	**1041.17**

D. Comparison with State-of-the-Art Methods

In this section, we conduct a comprehensive comparison of our proposed method against a wide range of 19 other RUL prediction techniques. These baseline methods are from six different categories:

- Traditional Machine Learning (ML) Methods: Support Vector Regression (SVR) [42], Random Forest (RF) [42], Gradient Boosting (GB) [42]
- CNN based Methods: one-dimensional Convolutional Neural Networks (1D-CNN) [15], two-dimensional Convolutional Neural Networks (2D-CNN) [42], Multi-Head Networks (MHN) [32]
- RNN based Methods: Long Short-Term Memory networks (LSTM) [43], Bidirectional LSTM (BiLSTM) [44], Bidirectional GRU Autoencoder (BiGRUAE) [45]
- CNN-RNN Hybrid Methods: hybrid CNN-LSTM [46], hybrid CNN-BiLSTM [47], Dual Attention Temporal Convolutional Network (DATCN) [4], hybrid 1D-CNN-BiGRU [31], Attention Guided CNN (AGCNN) [48]
- Transformer based Methods: Gated Convolutional Transformer (GCT) [33], Dual Aspect Self-Attention Based Transformer (DAST) [38], BiLSTM Denoising Autoencoder Transformer (BiLSTM-DAE Transformer) [40], Two-Stage Attention Based Hierarchical Transformer (STAR) [39]
- Graph Neural Network (GNN) based Methods: Spatial-Temporal Fusion Attention (STFA) [7], and Comprehensive Dynamic Structure GNN (CDSG) [49]

Table III and Table IV shows the comparison results in terms of RMSE and Score evaluation metric respectively.

From Table III, it is evident that our proposed PerFormer framework outperforms other state-of-the-art RUL prediction methods in terms of RMSE. While the improvements for FD001 and FD003 datasets are relatively modest (0.6% for FD001 and 3.9% for FD003), the enhancements for the more challenging FD002 and FD004 datasets, which feature a greater number of operational conditions, are significant. Specifically, PerFormer demonstrates an 8.4% improvement for the FD002 dataset and a remarkable 13.1% improvement for the FD004 dataset over the second-best RUL prediction model. Regarding the Score metric showed in Table IV, although our PerFormer framework achieves the second-best performance in most cases (FD001, FD002, and FD003), the differences from the top-performing algorithm are marginal. For instance, the best model for the FD001 dataset, BiLSTM-DAE Transformer, scores 169, while our PerFormer method achieves a score of 171.77, representing only a 0.59% difference. However, for the FD004 dataset, PerFormer significantly reduces the score from 1490 of the second-best DAST model to 1041.17, marking a substantial 30.1% improvement. These results illustrate that the permutation-enabled vision transformer effectively captures subtle features associated with the underlying engine degradation process and exhibits strong capabilities in modeling complex multivariate time series data. Consequently, it holds promising potential for practical condition-based maintenance systems. In our later ablation study, we will demonstrate the importance of both the permutation learning component and the vision transformer component of PerFormer in attaining these remarkable performance results.

E. Detailed Analysis of PerFormer

To evaluate the performance of our PerFormer framework for aircraft engines across different life cycle stages, we provide a detailed visual comparison between the predicted RULs generated by our model and the ground truth RULs across the FD001 to FD004 testing datasets in Figure 7. The x-axis in Figure 7 represents the Engine Unit Index, while the y-axis illustrates the RUL. Test sequences are organized

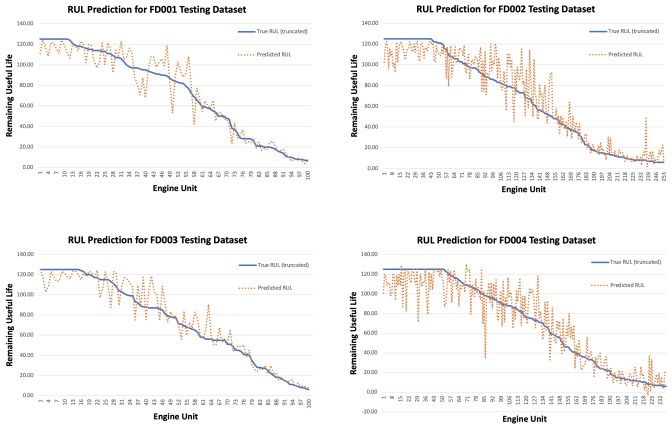

Fig. 7. Results for Comparing Estimated RUL and Actual RUL

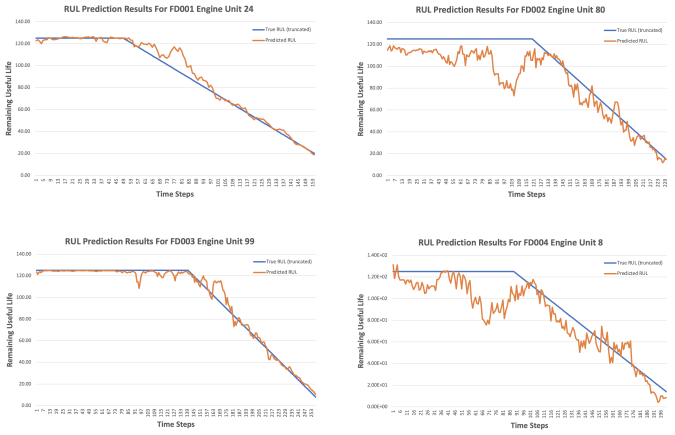

Fig. 8. Results for Comparing Estimated RUL and Actual RUL for Individual Test Unit

along the x-axis in ascending order based on their ground truth RUL to ensure clear visualization. It's notable that our model demonstrates significant precision, particularly for scenarios with smaller ground truth RULs (below 60), evident in FD001 and FD003 datasets. While a similar behavior is observed for FD002 and FD004 datasets, where the model exhibits substantial precision for smaller ground truth RULs, the threshold for achieving this precision is around 30, nearly 50% smaller compared to FD001 and FD003 datasets. This indicates that our model accurately predicts RUL over a wider range of aircraft engine life cycle stages for FD001 and FD003 datasets compared to FD002 and FD004 datasets. Additionally, there is a noticeable level of noise in the prediction results for FD002 and FD004 datasets compared to the smoother outcomes observed in FD001 and FD003. These differences may stem from variations in operational complexities, including the number of operating conditions and fault modes, as well as the size of the training dataset.

For a more detailed analysis of our PerFormer model's prediction results, we conduct a fine-grained examination by visually comparing the predicted RULs with the actual RULs of selected engine units from each of the four C-MAPSS

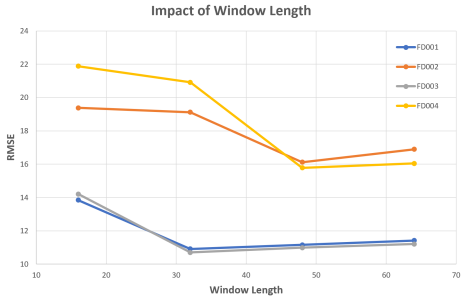

Fig. 9. Impact of Window Length for PerFormer

datasets. Figure 8 illustrates the RUL prediction outcomes for these engine test units across their operational life cycles. In our analysis, we select engine test units based on the selections provided by DAST [38] . Specifically, for FD001, we choose unit 24; for FD002, unit 80; for FD003, unit 99; and for FD004, unit 8. From Figure 8, it is evident that our PerFormer framework effectively predicts the RULs of test units in FD001 and FD003 datasets across various life cycle stages, spanning from the initial stage to the degradation stage. However, for the test units in FD002 and FD004 datasets, particularly during the initial stage with constant RUL, the PerFormer model demonstrates suboptimal prediction performance, tending to underestimate the RULs. Nevertheless, as the test units progress into the degradation stage, the predicted RULs by our PerFormer model closely align with the true RULs. This observation underscores the model's capability to accurately capture the degradation behavior of the engines based on the monitored data.

The window length is a critical factor in RUL prediction, directly impacting the temporal information available to the predictive model. Shorter windows may capture only a limited portion of the degradation trajectory, while longer windows could introduce noise or irrelevant data. To investigate the impact of window size, we assess the prediction performance of PerFormer in terms of RMSE using different window sizes: 16, 32, 48, and 64. The results, depicted in Figure 9, reveal insights into the model's performance across various datasets. In FD001 and FD003 datasets, smaller window sizes, such as 16, lead to suboptimal prediction performance, while increasing the window length to 32 improves model accuracy. However, further increasing the window size to 48 and 64 yields slightly diminished performance, likely due to noise within longer sequences. Conversely, for FD002 and FD004, smaller window sizes (16 and 32) result in suboptimal performance, attributed to the datasets' complexity. Optimal prediction performance is achieved with a window size of 48, whereas further increases to 64 lead to slight performance degradation due to noise in longer sequences.

F. Ablation Study

We also carried out a series of ablation studies to assess the impact of individual components within our PerFormer framework. The focus was on two main elements: the permutation matrix and the vision transformer. For this purpose, we

TABLE V
ABLATION STUDY FOR PERFORMER ON FD004

Method	RMSE	Score
Full PerFormer	15.78	1041.17
PerFormer w/o Permutation	18.21	2773.28
PerFormer w/o ViT	25.98	6129.03

executed two distinct experiments: one with the PerFormer framework without the permutation matrix learning component, and another with the vision transformer component removed. It's important to note that the PerFormer framework without the permutation matrix is effectively equivalent to a vanilla vision transformer. In the version without the vision transformer, this component is substituted with a CNN. These experiments were conducted using the FD004 dataset, and the results are presented in Table V. The findings indicate that the full PerFormer setup outperforms the basic vision transformer configuration, highlighting the beneficial role of the permutation matrix in enhancing feature representation learning, which subsequently improves prediction accuracy. Conversely, replacing the vision transformer with a CNN significantly worsens performance, underscoring the effectiveness of the vision transformer component.

V. CONCLUSION

In this study, we introduce PerFormer, a novel deep learning method for predicting RUL. The PerFormer model processes multivariate time series signals as row-wise permuted images, incorporating a permutation learning module alongside a vision transformer module. Specifically, we develop an innovative penalty function with a dynamic weight adjustment mechanism to facilitate permutation matrix learning. This technique rearranges the input data into an optimized 'image' format, which is then efficiently processed by the vision transformer module. Employing the CMAPSS dataset, our numerical experiments and ablation studies underscore the critical roles of both the permutation learning and the vision transformer components in RUL prediction. Remarkably, PerFormer achieves substantial performance enhancements over leading models, reducing the RMSE by 8.4% and 13.1% on the challenging FD002 and FD004 datasets, respectively. Furthermore, in the Score metric, PerFormer surpasses the top-performing existing method by 30.1% on the FD004 dataset. These results highlight the remarkable capability of the PerFormer framework to deliver accurate and reliable predictions of RUL, representing a significant advancement in aircraft engine prognostics and health management.

REFERENCES

[1] Z. Fan, K. Chang, R. Ji, and G. Chen, "Data fusion for optimal condition-based aircraft fleet maintenance with predictive analytics," *J. Adv. Inf. Fusion*, 2023.

[2] W. Mao, J. He, and M. J. Zuo, "Predicting remaining useful life of rolling bearings based on deep feature representation and transfer learning," *IEEE Transactions on Instrumentation and Measurement*, vol. 69, no. 4, pp. 1594–1608, 2019.

[3] H. Zhao, H. Liu, Y. Jin, X. Dang, and W. Deng, "Feature extraction for data-driven remaining useful life prediction of rolling bearings," *IEEE Transactions on Instrumentation and Measurement*, vol. 70, pp. 1–10, 2021.

[4] Y. Cheng, J. Wu, H. Zhu, S. W. Or, and X. Shao, "Remaining useful life prognosis based on ensemble long short-term memory neural network," *IEEE Transactions on Instrumentation and Measurement*, vol. 70, pp. 1–12, 2020.

[5] H. Peng, B. Jiang, Z. Mao, and S. Liu, "Local enhancing transformer with temporal convolutional attention mechanism for bearings remaining useful life prediction," *IEEE Transactions on Instrumentation and Measurement*, 2023.

[6] C. Chen, N. Lu, B. Jiang, Y. Xing, and Z. H. Zhu, "Prediction interval estimation of aeroengine remaining useful life based on bidirectional long short-term memory network," *IEEE Transactions on Instrumentation and Measurement*, vol. 70, pp. 1–13, 2021.

[7] Z. Kong, X. Jin, Z. Xu, and B. Zhang, "Spatio-temporal fusion attention: A novel approach for remaining useful life prediction based on graph neural network," *IEEE Transactions on Instrumentation and Measurement*, vol. 71, pp. 1–12, 2022.

[8] Y. Ding and M. Jia, "Convolutional transformer: An enhanced attention mechanism architecture for remaining useful life estimation of bearings," *IEEE Transactions on Instrumentation and Measurement*, vol. 71, pp. 1–10, 2022.

[9] X.-S. Si, W. Wang, C.-H. Hu, D.-H. Zhou, and M. G. Pecht, "Remaining useful life estimation based on a nonlinear diffusion degradation process," *IEEE Transactions on reliability*, vol. 61, no. 1, pp. 50–67, 2012.

[10] A. Ray and S. Tangirala, "Stochastic modeling of fatigue crack dynamics for on-line failure prognostics," *IEEE Transactions on Control Systems Technology*, vol. 4, no. 4, pp. 443–451, 1996.

[11] W. Li, J. Lee, J. Purl, F. Greitzer, B. Yousefi, and K. Laskey, "Experimental investigation of demographic factors related to phishing susceptibility," 2020.

[12] F. L. Greitzer, W. Li, K. B. Laskey, J. Lee, and J. Purl, "Experimental investigation of technical and human factors related to phishing susceptibility," *ACM Transactions on Social Computing*, vol. 4, no. 2, pp. 1–48, 2021.

[13] Z. Fan, W. Li, K. B. Laskey, and K.-C. Chang, "Investigation of phishing susceptibility with explainable artificial intelligence," *Future Internet*, vol. 16, no. 1, p. 31, 2024.

[14] W. Li, M. M. Finsa, K. B. Laskey, P. Houser, and R. Douglas-Bate, "Groundwater level prediction with machine learning to support sustainable irrigation in water scarcity regions," *Water*, vol. 15, no. 19, p. 3473, 2023.

[15] X. Li, Q. Ding, and J.-Q. Sun, "Remaining useful life estimation in prognostics using deep convolution neural networks," *Reliability Engineering & System Safety*, vol. 172, pp. 1–11, 2018.

[16] J. Zhu, N. Chen, and W. Peng, "Estimation of bearing remaining useful life based on multiscale convolutional neural network," *IEEE Transactions on Industrial Electronics*, vol. 66, no. 4, pp. 3208–3216, 2018.

[17] B. Yang, R. Liu, and E. Zio, "Remaining useful life prediction based on a double-convolutional neural network architecture," *IEEE Transactions on Industrial Electronics*, vol. 66, no. 12, pp. 9521–9530, 2019.

[18] H. Cheng, X. Kong, G. Chen, Q. Wang, and R. Wang, "Transferable convolutional neural network based remaining useful life prediction of bearing under multiple failure behaviors," *Measurement*, vol. 168, p. 108286, 2021.

[19] F. Jiang, K. Ding, G. He, H. Lin, Z. Chen, and W. Li, "Dual-attention-based multiscale convolutional neural network with stage division for remaining useful life prediction of rolling bearings," *IEEE Transactions on Instrumentation and Measurement*, vol. 71, pp. 1–10, 2022.

[20] B. Wang, Y. Lei, N. Li, and T. Yan, "Deep separable convolutional network for remaining useful life prediction of machinery," *Mechanical systems and signal processing*, vol. 134, p. 106330, 2019.

[21] T. S. Kim and S. Y. Sohn, "Multitask learning for health condition identification and remaining useful life prediction: deep convolutional neural network approach," *Journal of Intelligent Manufacturing*, vol. 32, no. 8, pp. 2169–2179, 2021.

[22] G. Mazaev, G. Crevecoeur, and S. Van Hoecke, "Bayesian convolutional neural networks for remaining useful life prognostics of solenoid valves with uncertainty estimations," *IEEE Transactions on Industrial Informatics*, vol. 17, no. 12, pp. 8418–8428, 2021.

[23] X. Xu, Q. Wu, X. Li, and B. Huang, "Dilated convolution neural network for remaining useful life prediction," *Journal of Computing and Information Science in Engineering*, vol. 20, no. 2, p. 021004, 2020.

[24] G. S. Chadha, U. Panara, A. Schwung, and S. X. Ding, "Generalized dilation convolutional neural networks for remaining useful lifetime estimation," *Neurocomputing*, vol. 452, pp. 182–199, 2021.
[25] A. Dosovitskiy, L. Beyer, A. Kolesnikov, D. Weissenborn, X. Zhai, T. Unterthiner, M. Dehghani, M. Minderer, G. Heigold, S. Gelly *et al.*, "An image is worth 16x16 words: Transformers for image recognition at scale," *arXiv preprint arXiv:2010.11929*, 2020.
[26] A. Vaswani, N. Shazeer, N. Parmar, J. Uszkoreit, L. Jones, A. N. Gomez, Ł. Kaiser, and I. Polosukhin, "Attention is all you need," *Advances in neural information processing systems*, vol. 30, 2017.
[27] P. Dierickx, A. Van Damme, N. Dupuis, and O. Delaby, "Comparison between cnn, vit and cct for channel frequency response interpretation and application to g. fast," *IEEE Access*, vol. 11, pp. 24 039–24 052, 2023.
[28] A. B. Amjoud and M. Amrouch, "Object detection using deep learning, cnns and vision transformers: a review," *IEEE Access*, 2023.
[29] M. D. Zeiler and R. Fergus, "Visualizing and understanding convolutional networks," in *Computer Vision–ECCV 2014: 13th European Conference, Zurich, Switzerland, September 6-12, 2014, Proceedings, Part I 13*. Springer, 2014, pp. 818–833.
[30] J. Ma, Y. Bai, B. Zhong, W. Zhang, T. Yao, and T. Mei, "Visualizing and understanding patch interactions in vision transformer," *IEEE Transactions on Neural Networks and Learning Systems*, 2023.
[31] J. Zhang, J. Tian, M. Li, J. I. Leon, L. G. Franquelo, H. Luo, and S. Yin, "A parallel hybrid neural network with integration of spatial and temporal features for remaining useful life prediction in prognostics," *IEEE Transactions on Instrumentation and Measurement*, vol. 72, pp. 1–12, 2022.
[32] L. Ren, H. Qin, Z. Xie, B. Li, and K. Xu, "Aero-engine remaining useful life estimation based on multi-head networks," *IEEE Transactions on Instrumentation and Measurement*, vol. 71, pp. 1–10, 2022.
[33] Y. Mo, Q. Wu, X. Li, and B. Huang, "Remaining useful life estimation via transformer encoder enhanced by a gated convolutional unit," *Journal of Intelligent Manufacturing*, vol. 32, no. 7, pp. 1997–2006, 2021.
[34] L. Ren, H. Wang, and G. Huang, "Dlformer: A dynamic length transformer-based network for efficient feature representation in remaining useful life prediction," *IEEE transactions on neural networks and learning systems*, 2023.
[35] Y. Zhang, C. Su, J. Wu, H. Liu, and M. Xie, "Trend-augmented and temporal-featured transformer network with multi-sensor signals for remaining useful life prediction," *Reliability Engineering & System Safety*, vol. 241, p. 109662, 2024.
[36] Y. Li, Y. Chen, H. Shao, and H. Zhang, "A novel dual attention mechanism combined with knowledge for remaining useful life prediction based on gated recurrent units," *Reliability Engineering & System Safety*, vol. 239, p. 109514, 2023.
[37] F. Xiang, Y. Zhang, S. Zhang, Z. Wang, L. Qiu, and J.-H. Choi, "Bayesian gated-transformer model for risk-aware prediction of aero-engine remaining useful life," *Expert Systems with Applications*, vol. 238, p. 121859, 2024.
[38] Z. Zhang, W. Song, and Q. Li, "Dual-aspect self-attention based on transformer for remaining useful life prediction," *IEEE Transactions on Instrumentation and Measurement*, vol. 71, pp. 1–11, 2022.
[39] Z. Fan, W. Li, and K.-C. Chang, "A two-stage attention-based hierarchical transformer for turbofan engine remaining useful life prediction," *Sensors*, vol. 24, no. 3, p. 824, 2024.
[40] ——, "A bidirectional long short-term memory autoencoder transformer for remaining useful life estimation," *Mathematics*, vol. 11, no. 24, p. 4972, 2023.
[41] D. Chen, W. Hong, and X. Zhou, "Transformer network for remaining useful life prediction of lithium-ion batteries," *Ieee Access*, vol. 10, pp. 19 621–19 628, 2022.
[42] G. Sateesh Babu, P. Zhao, and X.-L. Li, "Deep convolutional neural network based regression approach for estimation of remaining useful life," in *Database Systems for Advanced Applications: 21st International Conference, DASFAA 2016, Dallas, TX, USA, April 16-19, 2016, Proceedings, Part I 21*. Springer, 2016, pp. 214–228.
[43] S. Zheng, K. Ristovski, A. Farahat, and C. Gupta, "Long short-term memory network for remaining useful life estimation," in *2017 IEEE international conference on prognostics and health management (ICPHM)*. IEEE, 2017, pp. 88–95.
[44] J. Wang, G. Wen, S. Yang, and Y. Liu, "Remaining useful life estimation in prognostics using deep bidirectional lstm neural network," in *2018 Prognostics and System Health Management Conference (PHM-Chongqing)*. IEEE, 2018, pp. 1037–1042.
[45] Y. Duan, H. Li, M. He, and D. Zhao, "A bigru autoencoder remaining useful life prediction scheme with attention mechanism and skip connection," *IEEE Sensors Journal*, vol. 21, no. 9, pp. 10 905–10 914, 2021.
[46] Z. Kong, Y. Cui, Z. Xia, and H. Lv, "Convolution and long short-term memory hybrid deep neural networks for remaining useful life prognostics," *Applied Sciences*, vol. 9, no. 19, p. 4156, 2019.
[47] H. Liu, Z. Liu, W. Jia, and X. Lin, "A novel deep learning-based encoder-decoder model for remaining useful life prediction," in *2019 International Joint Conference on Neural Networks (IJCNN)*. IEEE, 2019, pp. 1–8.
[48] Y. Song, S. Gao, Y. Li, L. Jia, Q. Li, and F. Pang, "Distributed attention-based temporal convolutional network for remaining useful life prediction," *IEEE Internet of Things Journal*, vol. 8, no. 12, pp. 9594–9602, 2020.
[49] H. Wang, Z. Zhang, X. Li, X. Deng, and W. Jiang, "Comprehensive dynamic structure graph neural network for aero-engine remaining useful life prediction," *IEEE Transactions on Instrumentation and Measurement*, 2023.